Theoretical and Applied Fracture Mechanics 117 (2022) 103204

Contents lists available at ScienceDirect

Theoretical and Applied Fracture Mechanics

journal homepage: www.elsevier.com/locate/tafmec

Fracture and deformation behaviors of saturated and dried single-edge notched beam sandstones under three-point bending based on DIC

Xiaofeng Qin [a], Haijian Su [a,b,*], Yujie Feng [a], Honghui Zhao [a,c], Thi Nhan Pham [d]

[a] State Key Laboratory for Geomechanics and Deep Underground Engineering, China University of Mining and Technology, Xuzhou 221116, China
[b] State Key Laboratory of Coking Coal Exploitation and Comprehensive Utilization, China Pingmei Shenma Group, Pingdingshan 467000, China
[c] East China Environmental Geotechnical Branch, China Petroleum Engineering Construction Company, Qingdao 266000, China
[d] Faculty of Civil Engineering, Hanoi University of Mining and Geology, Hanoi 100000, Viet Nam

ARTICLE INFO

Keywords:
Mixed mode I-II fracture
Moisture condition
DIC
Fracture toughness
Maximum principal strain field

ABSTRACT

It is of great significance to study the fracture and deformation characteristics of rock with different moisture conditions for the safety assessment of "fragile surface with cracks" in rock engineering such as dams and underground chambers affected by groundwater. Therefore, in this work, three-point bending tests were conducted on single-edge notched beam sandstone specimens with different moisture conditions (natural condition, dried condition, and saturated condition) under complex stress environment. Additionally, the digital image correlation (DIC) method was used to quantitatively research the fracture parameters and deformation behavior of specimens during pure mode I fracture and mixed mode I-II fracture. The results show that (1) the average peak load of dried sandstone is 42.18–116.08% higher than that of saturated sandstone. (2) By increasing the offset distance of the pre-notch (0–72 mm), the specimen is transformed from pure mode I fracture to mixed mode I-II fracture, with an increase in average peak load of 152.83–284.24%. (3) When the pure mode I fracture occurs in saturated sandstone, the fracture toughness is 66.74% of that natural sandstone, which is 46.28% of that dried sandstone. (4) In the mixed mode I-II fracture, the effective fracture toughness of sandstone with a consistent moisture condition is 1.05–1.70 times that of the pure mode I fracture. (5) The fracture toughness of saturated sandstone is most significantly affected by the loading mode. When the offset distance of pre-notch increases from 0 to 72 mm, the average effective fracture toughness increases from 4.324 MPa·mm$^{0.5}$ to 7.357 MPa·mm$^{0.5}$, increasing by 70.14%. Besides, according to the trend of the *ap*, which was calculated by the DIC method, the post-peak macroscopic crack propagation is divided into two stages: the post-peak stable propagation stage and the post-peak unstable propagation stage.

1. Introduction

In rock engineering such as mines, tunnels, underground chambers, and dams [1,2], groundwater and surface water have a great influence on the strength and deformation performance of surrounding rock masses. The change in water content of rock may affect the strength and deformation performance of the rock. The researchers have conducted a series of experiments to study the influence of moisture conditions on the mechanical properties of rock. For instance, Li et al. [3] discussed the influence of water content on the strength and deformability of two *meta*-sedimentary rocks by triaxial compressive tests. The results showed that although the water content of the two tested rocks is very low, it has a significant weakening effect on the triaxial compressive strength. By conducting laboratory tests on five kinds of rocks, Hashiba and Fukui [4] found that the water-bearing rocks are not only compressive strength, but also uniaxial tensile strength of are lower than those of dry rock. In addition, the reduction rate of uniaxial tensile strength is greater than that of compressive strength. Zhou et al. [5] carried out dynamic and static tests on water-bearing sandstone to measure the tensile and compressive strength, and found that the retarding effect of water on crack was not obvious. Due to the high strain rate of loading conditions, dynamic cracks expand fast, and water fails to reach the crack tip. Erguler and Ulusay [6] measured the uniaxial compressive strength, tensile strength, and modulus of elasticity of

* Corresponding author at: State Key Laboratory for Geomechanics and Deep Underground Engineering, China University of Mining and Technology, Xuzhou 221116, China.
E-mail address: hjsu@cumt.edu.cn (H. Su).

https://doi.org/10.1016/j.tafmec.2021.103204
Received 22 July 2021; Received in revised form 26 November 2021; Accepted 29 November 2021
Available online 7 December 2021

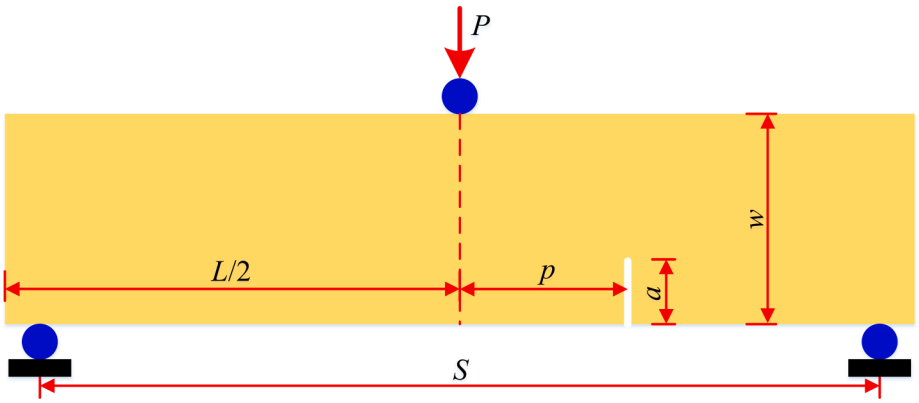

Fig. 1. Simplified model of three-point bending test for SENB specimen.

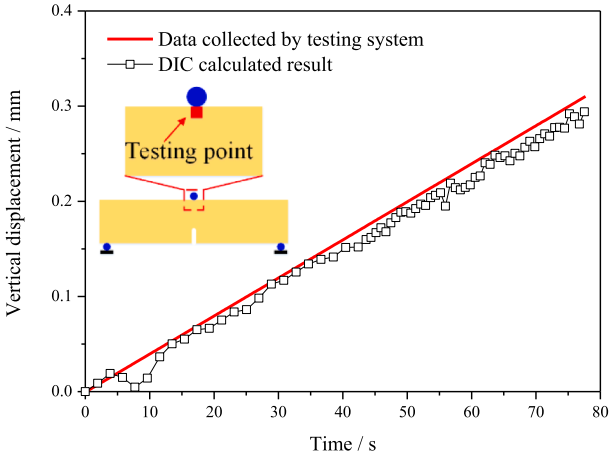

Fig. 2. Comparison between the axial displacement from DIC and the loading curve of loading system.

numerous specimens with different water contents. The results likewise showed that with the increase of the water content, the reductions in the uniaxial compressive strength and tensile strength are up to 90% from oven-dried to saturated conditions. Moreover, the elastic modulus of the specimens also decreases by 93%.

Due to geological and tectonic effects, there are many defects in rock masses, such as joints, cracks, holes, and so on [7–9]. The existence of these defects destroys the structural integrity of rocks, and the propagation of cracks also has an important impact on the mechanical properties of rocks. In laboratory tests, small notches are often prefabricated on specimens to study the fracture properties of rocks. Xi et al. [10] observed that, for pre-cracked specimens, crack initiation and propagation will occur when the stress is far less than the compressive strength. Yang et al. [11] conducted uniaxial compression tests on brittle sandstone specimens containing a single fissure. It was found that the compressive strength, Young's modulus and peak axial strain of sandstone specimens with pre-existing single fissure are all lower than that of intact sandstone specimen, which is closely related to the fissure length and fissure angle. During direct tensile testing (DTT) and uniaxial compression testing (UCT), Liu [12] found that the strengths of the single-cracked cylindrical sandstone with pre-crack dip angle of 0-90° decrease with the decrease of dip angle. The weakening degree varies from 63.66% to 4.10% in DTT and from 67.53% to 8.61% in UCT. Apart from the above tests, numerous tests were conducted to study the fracture behavior of rocks by using specimens containing pre-crack [13–14].

The initiation of macrocracks is not an abrupt behavior but a cumulative damage process [15]. In previous work [16–18], high-resolution digital cameras, and high-speed recording cameras were often used to record the evolution of cracks. However, in some cases, even if the camera has a high-resolution and high zoom performance, some cracks are still not evident in the images, especially if the crack opening is smaller than the image pixel size. In recent years, the digital image correlation (DIC) method has been widely used in the study of rock deformation behavior and fracture characteristics due to its accuracy and convenience [19–20]. Yue et al. [21] used the DIC method and the strain gage method to perform dynamic three-point bending impact tests on the white marble specimens, and the results showed that the complete fracture process (including the variations in successive displacement and strain fields) can be obtained by the DIC method, while the strain gage method can only give a rough changing trend. Miao et al. [22] obtained the full-field deformation evolution of granite based on DIC method combined with acoustic emission characteristics, revealing the damage evolution and fracture mechanism of heated granite.

The fracture modes can be divided into three basic modes according to the characteristics of stress and displacement, namely, opening or tensile mode (Mode I), sliding mode (Mode II), and tearing mode (Mode III) [23]. A large number of single-model fracture processes have been studied [24–26]. In fact, the rock is usually in a complex stress state, and the cracks generated in the plane often show mixed mode I-II. Therefore, three-point bending (TPB) tests were conducted on single-edge notched beam (SENB) sandstones with different moisture conditions in this work. The variation of maximum principal strain field and the aperture of pre-notch under different loading modes were quantitatively analyzed by the DIC method. The deformation characteristics of cracks during fracture were revealed, and the post-peak fracture stage was further subdivided.

2. SENB specimen and testing method

2.1. Preparation of SENB specimen

The sandstone material used in this study has a bulk density of 2200 kg/m^3, which was collected from Linyi City, Shandong Province, China. The sandstone has no surface texture with the color of light yellow in natural state. The X-ray diffraction (XRD) results showed that the specimen is composed of 98.9% quartz and 1.1% clay minerals. The SENB specimens were prepared by wire electrical discharge machining (WEDM) cutting beams of 260 mm (length) * 60 mm (width) * 28.25 mm (thickness), as shown in Fig. 1. The length a and aperture of the pre-notch are 18 and 1 mm, respectively. In addition, the span S of the two fixed fulcrum points is 240 mm. Four different values for the pre-crack offset distances (p) were chosen: p = 0, 24, 48, and 72 mm, respectively. Different combinations of modes I and II can be provided by changing p. When the crack line is along the direction of applied load (p = 0), the SENB specimen is subjected to pure mode I (or pure opening

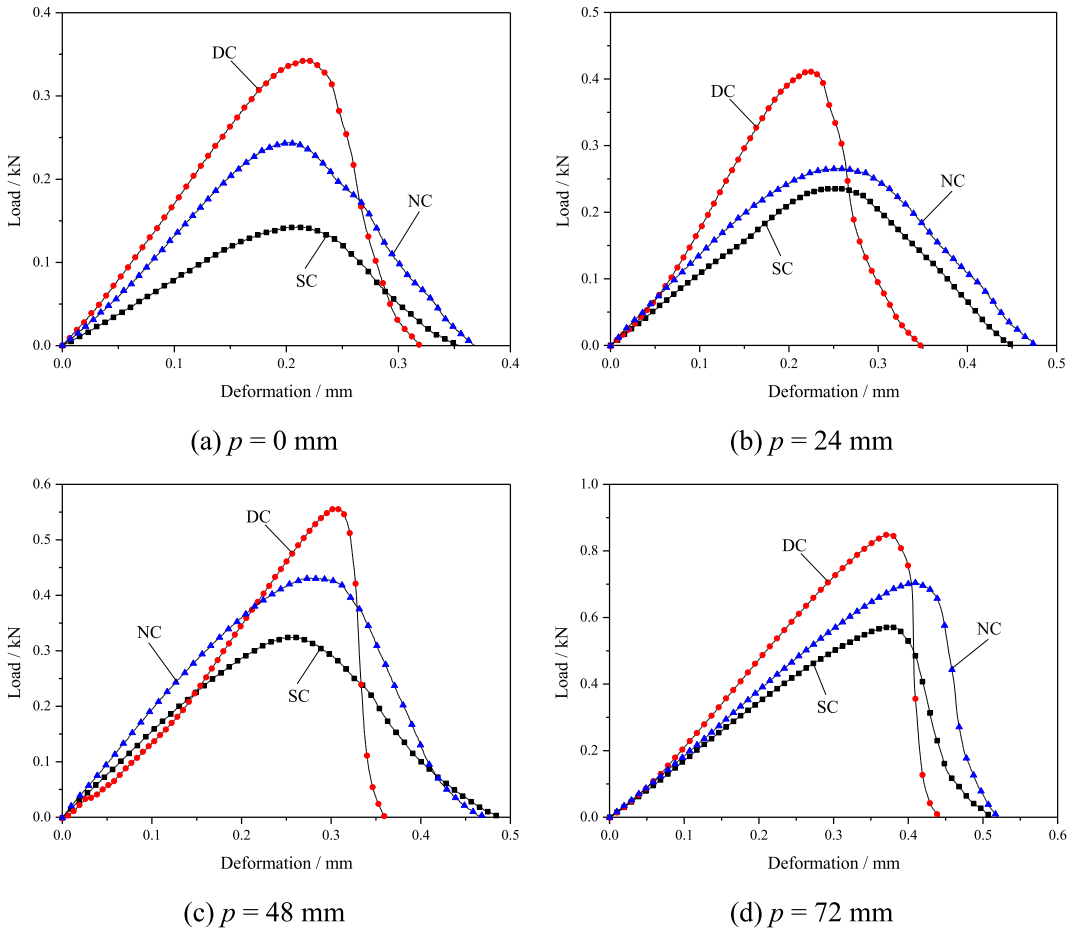

Fig. 3. Load-deformation curves of sandstone specimens with different notch offsets under TPB.

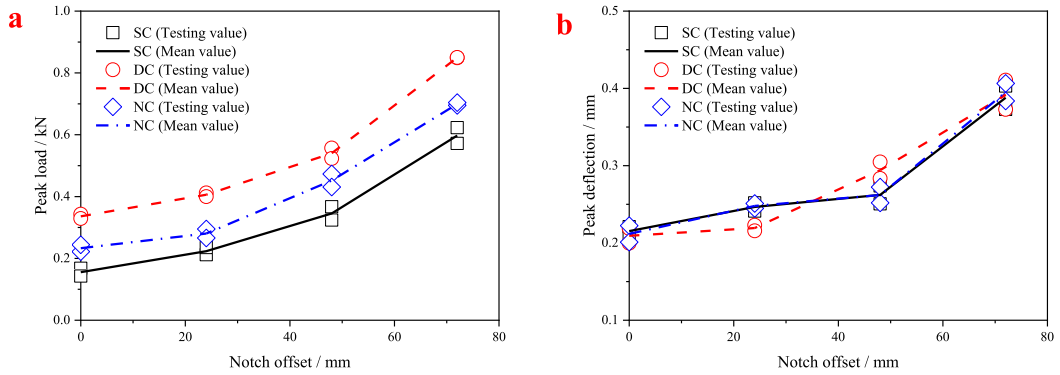

Fig. 4. Variations in (a) peak load and (b) peak deflection of SENB with different notch offsets.

mode) because of the geometry and loading symmetry with respect to the crack [27]. For nonzero pre-crack offset distances, mode II appears during the crack deformation.

To explore the influence of moisture condition on rock mechanical parameters and fracture characteristics, three conditions i.e. saturated condition (SC), dried condition (DC), and natural condition (NC) were selected. The specimens of the DC group and SC group were first placed in a drying box for 48 h at 105 °C. At this time, the quality of these specimens no longer changed. After the specimens were taken out and quickly weighed, the specimens of the DC group were sealed with preservative film immediately. The specimens of the SC group were saturated by the BH-I rock vacuum saturation test device, and the saturation time was 3 days under the condition of 0.5 MPa. Then the specimens were weighed. The NC group was weighed without special treatment. Two specimens were prepared in each group to reduce the experimental error. The water content of specimens in DC, NC, and SC was 0.00%, 0.75%, and 4.59%, respectively.

2.2. *Three-point bending testing method*

The CSS-44100 electronic universal testing machine, with a maximum test force of 200 kN, was used to conduct three-point bending tests on SENB specimens. The specimen was placed on two fixed fulcrum points at a span of 240 mm (Fig. 1). A line load was applied to the top center of the specimen. The displacement loading mode was used during the test with a constant loading rate of 0.2 mm/min. Besides, a high-

Table 1
Fracture parameters of sandstone specimens with different water contents in the process of mode I fracture and mixed mode I-II fracture under TPB.

No.	Condition	p/mm	$2p/S$	a/w	P_0 / kN	K_{If}/(MPa·mm$^{0.5}$)	K_{IIf}/(MPa·mm$^{0.5}$)	K_{eff}/(MPa·mm$^{0.5}$)
S05#	SC	0	0	0.3	0.168	4.671	0.000	4.671
S06#	SC	0	0	0.3	0.143	3.976	0.000	3.976
S11#	SC	24	0.2	0.3	0.212	5.135	0.427	5.153
S12#	SC	24	0.2	0.3	0.235	5.693	0.473	5.712
S17#	SC	48	0.4	0.3	0.367	6.653	0.809	6.702
S18#	SC	48	0.4	0.3	0.324	5.874	0.714	5.917
S23#	SC	72	0.6	0.3	0.623	7.568	1.252	7.671
S24#	SC	72	0.6	0.3	0.572	6.949	1.149	7.043
S03#	DC	0	0	0.3	0.343	9.537	0.000	9.537
S04#	DC	0	0	0.3	0.329	9.148	0.000	9.148
S09#	DC	24	0.2	0.3	0.412	9.980	0.830	10.015
S10#	DC	24	0.2	0.3	0.400	9.690	0.806	9.723
S15#	DC	48	0.4	0.3	0.557	10.098	1.228	10.172
S16#	DC	48	0.4	0.3	0.539	9.771	1.188	9.843
S21#	DC	72	0.6	0.3	0.849	10.314	1.706	10.454
S22#	DC	72	0.6	0.3	0.850	10.326	1.708	10.466
S01#	NC	0	0	0.3	0.222	6.173	0.000	6.173
S02#	NC	0	0	0.3	0.244	6.784	0.000	6.784
S07#	NC	24	0.2	0.3	0.295	7.146	0.594	7.171
S08#	NC	24	0.2	0.3	0.266	6.444	0.536	6.466
S13#	NC	48	0.4	0.3	0.473	8.575	1.042	8.638
S14#	NC	48	0.4	0.3	0.431	7.813	0.950	7.871
S19#	NC	72	0.6	0.3	0.695	8.443	1.397	8.558
S20#	NC	72	0.6	0.3	0.704	8.552	1.415	8.668

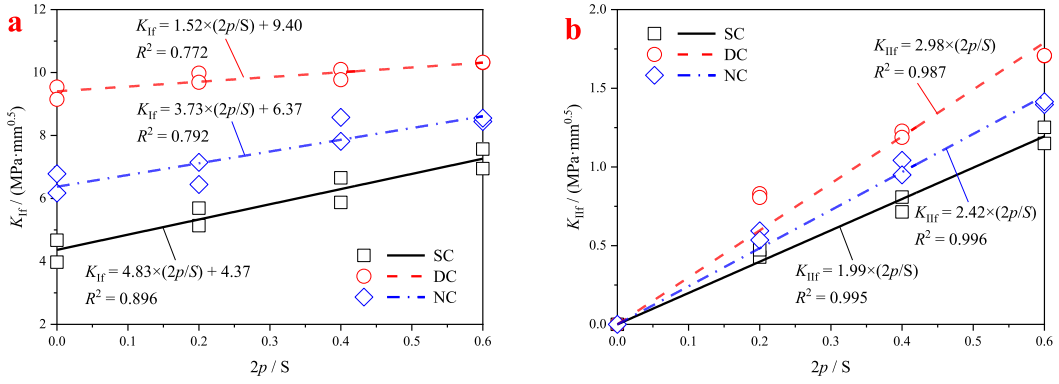

Fig. 5. Relationships of (a) K_{If} and (b) K_{IIf} with $2p/S$.

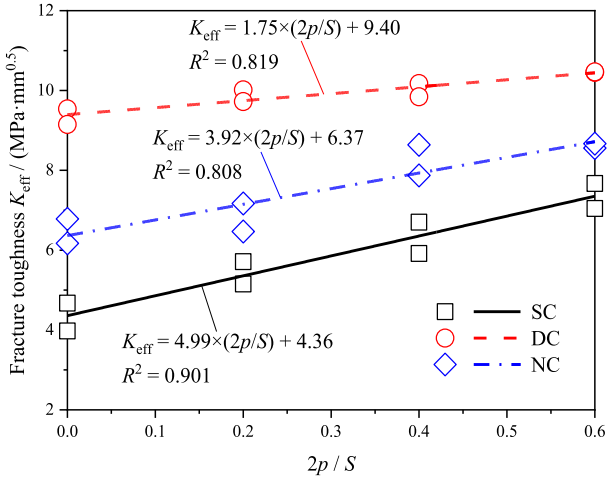

Fig. 6. Variation in fracture toughness of SENB under different conditions.

definition camera (Basler acA1600-20gm) was used to capture the specimen images with a resolution of 2048 * 2048 pixels at a speed of 5 frames per second during the whole loading test.

To certify the effectivity of DIC, the point on the specimen which is near the loading head was taken as the testing point. Fig. 2 shows the axial displacement of the landmark point of specimen S03# in the TPB loading process analyzed by the DIC. The displacement curve of the DIC shows a great similarity with that of the loading system. Although due to the hysteresis of surface deformation of rocks, the displacements analyzed by the DIC are slightly smaller than those automatically collected by the loading system. But the calculation results of the DIC can still effectively reflect the actual displacement situation.

3. Result analysis

3.1. Fracture characteristic

In Fig. 3a ~ d, the load-deformation curves of sandstone under TPB are plotted when the offset distances are 0, 24, 48, and 72 mm, respectively. At the initial stage of loading, the area near the loading head begins to be compacted at first. Due to insufficient contact among rock particles, the force transfer is relatively slow, which is manifested as slow deformation. The specimen shows linear elastic deformation with approximately linear curve growth after compaction. The ability to resist fracture rapidly decreases after peak load due to the germination and gradual nucleation of internal microcracks [28]. The rock continues to deform and fracture until it is completely fractured. It is worth noting

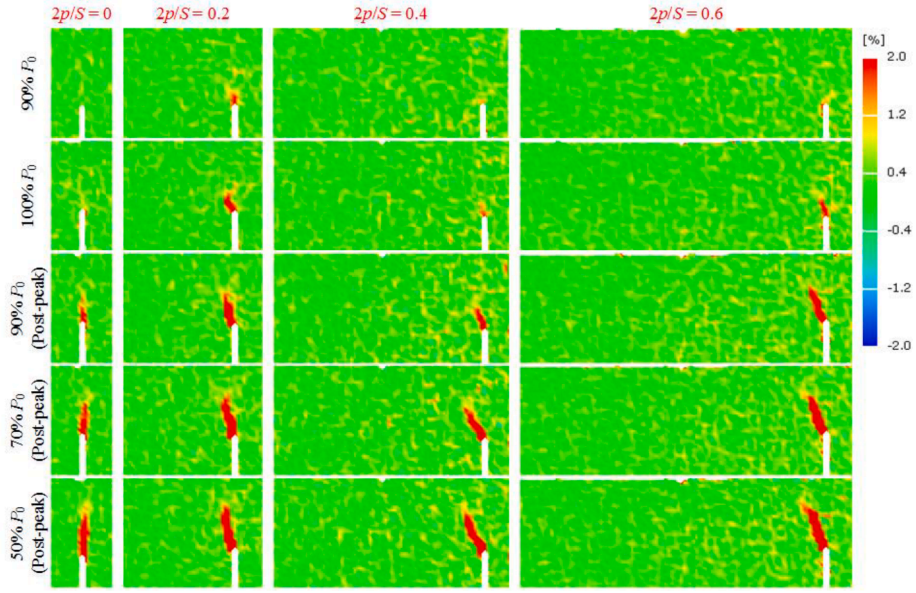

(a) SC

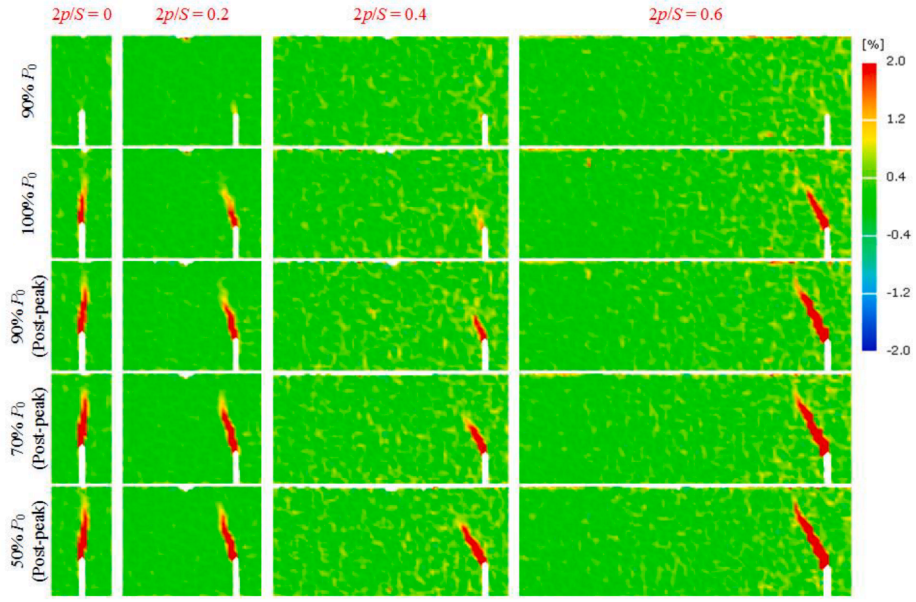

(b) DC

Fig. 7. Evolution processes of maximum principal strain field of sandstone specimens in (a) saturated and (b) dried conditions during loading process.

that the deformation variation of the pre-peak load is greater than that of the post-peak load. Cracks exist in the specimen as microcracks, and the specimen gradually deforms with the increase of load in the pre-peak stage. In the post-peak stage, the nucleation microcracks propagate and connect rapidly, forming obvious macroscopic cracks in the specimen. The macrocracks quickly penetrate the specimen, which destroy the continuity of the specimen structure. The specimen is completely destroyed, and the loading is over. It is precisely because the crack rapidly destroys the continuity of the specimen in the post-peak stage. The main means of releasing energy of the specimen in the post-peak stage are no longer in the form of deformation energy as in the pre-peak stage but in the form of fracture energy. It rapidly releases energy through fracture [29,30]. Besides, under the same loading mode, the moisture condition of the specimen also influences on the load-deformation relationship of the specimen. It is not difficult to see that the bearing capacity of sandstone in the pre-peak stage is the strongest under dried condition, followed by natural condition, and the weakest under saturated condition. In the post-peak stage, the dried sandstone shows stronger brittleness compared with the natural and saturated sandstone. The rapid decline of the bearing capacity in the post-peak stage reflects the brittleness of dried sandstone. Generally, compared with the dried sandstone, the brittleness of water-bearing sandstone and saturated sandstone gradually decreases while the ductility increases [31]. This ductility is mainly manifested in that the bearing capacity does not significantly decrease after the peak before the complete failure of the structure, and large deformation still occurs in the post-peak

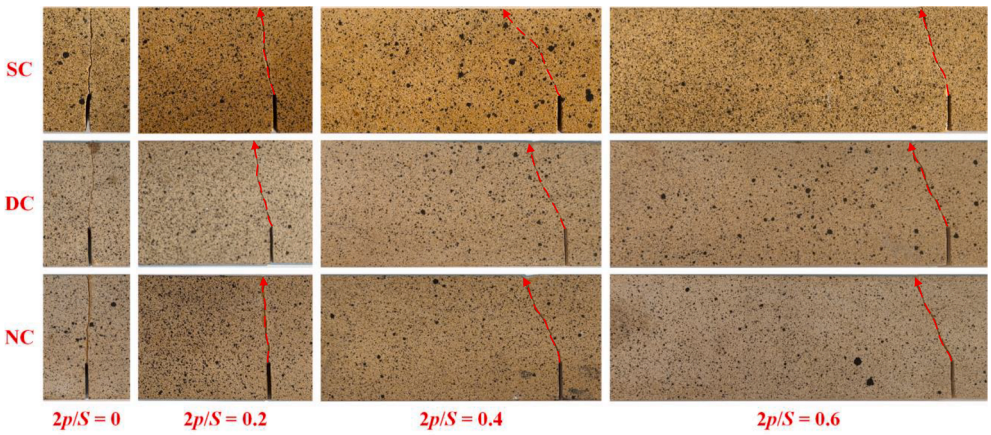

Fig. 8. Typical crack propagation path of SENB specimens under three-point bending test.

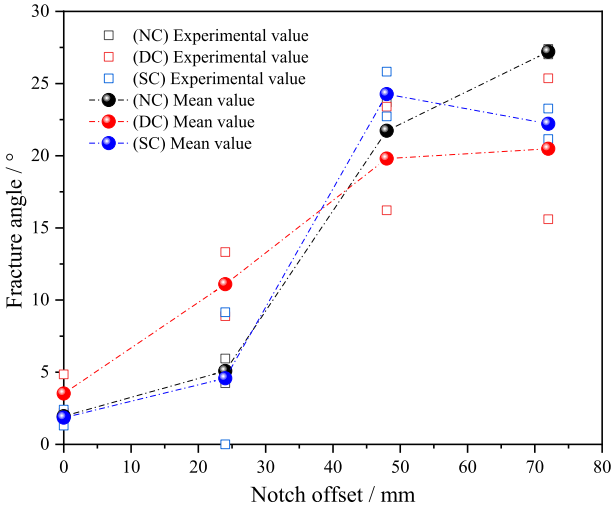

Fig. 9. Variation in fracture angle with notch offset.

stage. The plastic deformation is more significant for the wet specimens, and the yielding and failure processes for the dried specimens are faster and more violent [32].

To better study the influence of moisture condition and loading mode on the fracture properties of sandstone specimens, the peak load and peak deflection of each group of specimens were separately compared, as shown in Fig. 4, in which the peak deflection refers to the deflection corresponding to the time of peak load. It can be seen that both the peak load and peak deformation are affected by the loading mode, and increase with the increase of the notch offset. For example, when the notch offset of saturated sandstone increases from 0 to 72 mm, the average of peak load increases from 0.156 kN to 0.598 kN, and the average peak deflection increases from 0.215 mm to 0.39 mm. The increase of peak load is 283.3% while the increase of peak deflection is 81.4%. In addition, the peak load is related to different moisture conditions. When the notch offset is 48 mm, the average peak strength of sandstone in DC group, NC group, and SC group is 0.548, 0.451, and 0.346 kN, respectively. The peak load of sandstone is also affected by the fracture mode of pre-notch, and is more affected by fracture mode than by moisture condition. The average peak load of dried sandstone is 42.18–116.08% higher than that of saturated sandstone. By increasing the offset distance of the pre-notch (0–72 mm), the specimen is transformed from pure mode I fracture to mixed mode I-II fracture, and the average peak load of the specimen increases by 152.83%-284.24%. The weakening of rock strength by water is mainly caused by pore pressure, chemical and physical deterioration, capillary tension, and other factors [33,34]. However, the moisture condition has a little effect on the peak deflection. Although the peak load of the SC group is significantly smaller than that of the NC group, the value of peak deflection is extremely close in Fig. 4b. The peak deflection grows slowly at the notch offset of 0, 24, and 48 mm, while greatly increases at the notch offset of 72 mm. But the peak deflection of dried specimens increases significantly at the notch offset of 48 mm. It can be said that dried sandstone is more sensitive to the influence of notch offset on peak deflection.

Fracture toughness, a vital mechanics index, is often used to reflect the ability of rock to resist fracture. The stress intensity factors, K_I and K_{II}, which describe the local stress and strain field around the crack tip for mixed-mode loading can be expressed as follows [35]:

$$K_{If} = \sigma Y_I \sqrt{\pi a} \tag{1}$$

$$K_{IIf} = \sigma Y_{II} \sqrt{\pi a} \tag{2}$$

Where a is the notch depth, Y_I, Y_{II} are the dimensionless stress intensity factor under plane stress state. In this paper, the values of Y_I and Y_{II} are based on the data obtained by Fett [35]. The applied stress σ is given by:

$$\sigma = \frac{3PS}{2w^2 b} \tag{3}$$

Where P is the applied load, S is the span, and w and b are the specimen depth and width, respectively.

After the test, the stress intensity factors of each specimen were obtained by using the measured values substituted into Eqs. (1), (2), and (3) above. The detailed values were shown in Table 1.

The variation of the stress intensity factor of sandstone (NC, SC, and DC) with different offset distances of the pre-notch, as shown in Fig. 5. The K_{If} and K_{IIf} of each group of specimens decrease gradually with the increase of moisture. For example, when the offset distance of the pre-notch is 48 mm ($2p/S = 0.4$), the K_{If} of DC, NC, and SC groups are 10.036, 7.867, and 6.344 MPa·mm$^{0.5}$, respectively. The value of K_{IIf} of each group is 1.2 (DC), 0.974 (NC), and 0.799 (SC) MPa·mm$^{0.5}$, respectively. Besides, the stress intensity factors K_{If} and K_{IIf} of each group of specimens show an approximate linear growth trend. For example, in Fig. 5b, there is a good linear relationship between K_{IIf} and $2p/S$, and the fitting coefficients R^2 are 0.995 (SC), 0.996 (NC), and 0.987 (DC), respectively. It is noticeable that the mode I stress intensity factor range of mixed mode I-II fracture is 5.135–10.326 MPa·mm$^{0.5}$, while the mode II stress intensity factor range is 0.427–1.708 MPa·mm$^{0.5}$. The K_{If} of mixed mode I-II fracture under different notch offsets is always larger than K_{IIf}, which indicates that the shear stress field strength at the crack tip is greater than the tensile stress field strength when the load of the specimen reaches its peak value. That is, the mode I fracture is dominant in the mixed mode I-II fracture of rock.

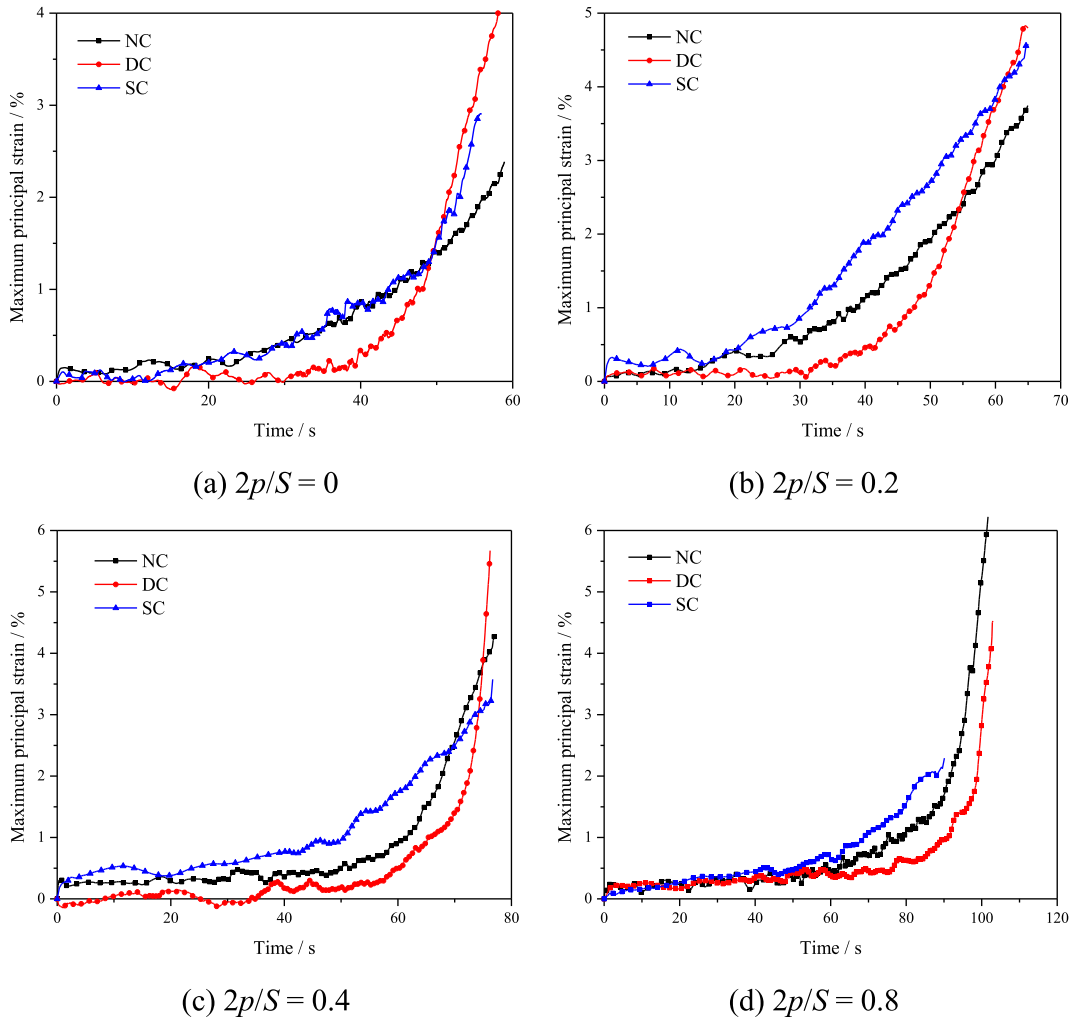

Fig. 10. The maximum principal strain at the pre-notch tip of sandstone in the loading process analyzed by DIC.

In general, the effective value of fracture toughness (K_{eff}) of mixed mode I-II fracture may be written in the following form:

$$K_{eff} = \sqrt{K_{If}^2 + K_{IIf}^2} \tag{4}$$

The variation in fracture toughness of SENB under different conditions is shown in Fig. 6. The K_{eff} decreases gradually with the increase of moisture. When the pure mode I fracture ($2p/S = 0$) occurs in saturated sandstone, the fracture toughness is 66.74% of that natural sandstone, which is 46.28% of that dried sandstone. When the value of pre-notch offset distance is 24 mm ($2p/S = 0.2$), the average effective fracture toughness of SENB specimen is 9.869 (DC), 6.819 (NC), and 5.433 MPa·mm$^{0.5}$ (SC), respectively. The tiny pores of saturated sandstone are filled with water molecules. Mineral particles pull surrounding water molecules using surface gravity, and the water molecules squeeze into the gap between particles due to attraction at the particle contact. The formation of the water wedge effect, resulting in reduced bonding force between mineral particles and friction, water plays a lubricating role [36]. In addition to water wedge effect, the softening of mineral particles and the weakening of intergranular connections also have an influence [37]. Furthermore, when the moisture content of dried sandstone increases gradually, the type of fracture transfers from the *trans*-granular fracture to inter-granular fracture [38]. Therefore, the ability of saturated sandstone to resist fracture is less than that of dried sandstone. Besides, the K_{eff} of specimens increases gradually with an increase in notch offset. The effective fracture toughness of sandstone with consistent moisture condition in the mixed mode I-II fracture is 1.05–1.70 times that of the pure mode I fracture. The fracture toughness of saturated sandstone is most significantly affected by the loading mode. As the notch offset rises from 0 to 72 mm, the average effective fracture toughness of saturated sandstone increases from 4.324 to 7.357 MPa·mm$^{0.5}$, with an increase extent of 70.14%. In other words, the ability of the specimen to resist mixed mode I-II fracture is greater than that to resist tensile fracture. Moreover, an increase of offset distance of pre-notch can reduce the influence of moisture condition on the fracture toughness of sandstone. When the notch offset increases from 0 mm to 48 mm ($2p/S = 0.4$), the difference between the average fracture toughness of saturated sandstone and that of dried sandstone is reduced by 26.32%.

3.2. Deformation feature

At present, acoustic emission (AE) monitoring, CT, and DIC are the main methods to study the process of crack germination and propagation. The AE monitoring can locate the moment of crack germination through energy, but it lacks intuitiveness. The CT operation is complicated, while DIC technology can identify damage evolution or crack propagation by obtaining the surface displacement field or strain field of the specimen through non-contact digital image information [39–41].

Fig. 7 provides the evolution processes of the maximum principal strain field around the pre-notch. When the axial load reaches 90% of the peak load, the strain concentration has already appeared on the tip of the pre-notch of the SC specimen, while there is no obvious strain

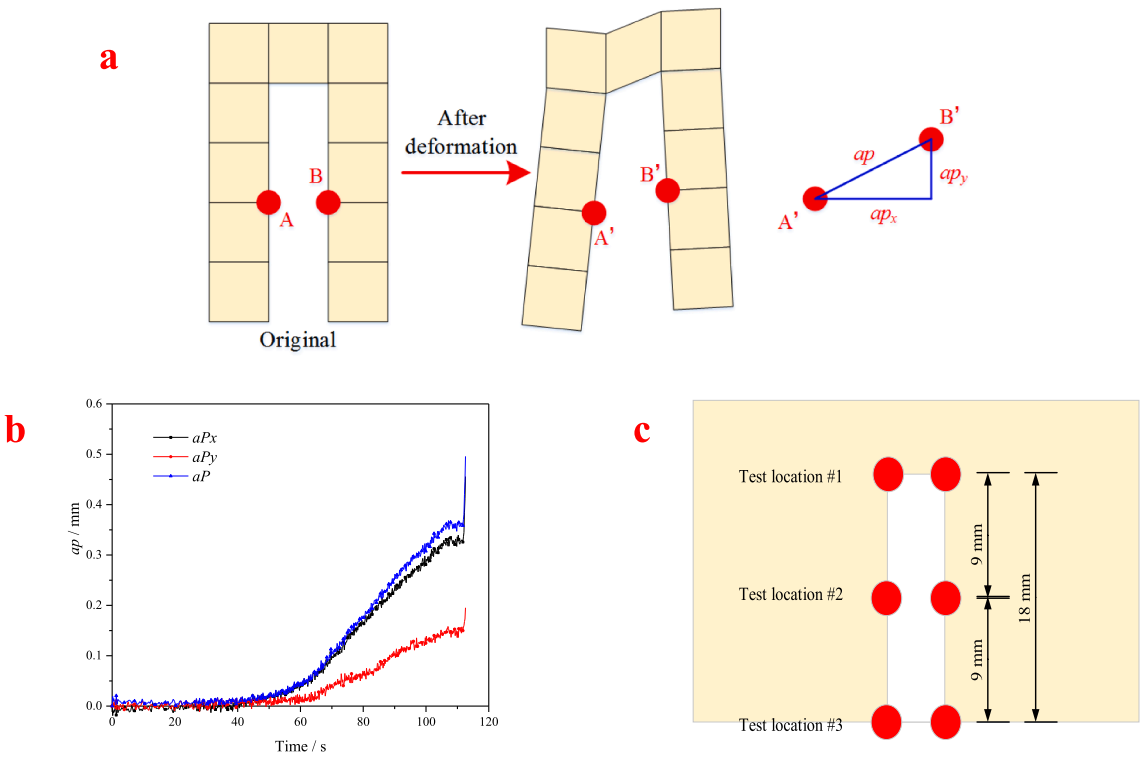

Fig. 11. (a) Schematic of aperture calculation between two points of pre-notch, (b) A typical curves of *apx*, *apy*, and *ap*, (c) The location of test point.

concentration on the tip of the pre-notch of the DC specimen. The area of obvious strain concentration in the DC specimen is larger than that in the SC specimen at peak load. Therefore, it can be considered that the DC specimen shows stronger resistance to cracks before the occurrence of obvious cracks compared with the SC specimen. The crack propagation of the DC specimen is faster and stronger after an obvious crack occurs. That is, the DC specimen shows strong brittleness after an obvious crack occurs. The region with obvious strain concentration continues to expand after the peak load, and the propagation path is basically consistent with the crack propagation path of the specimen in Fig. 8.

As seen from Fig. 8, the propagation direction of the pre-notch is related to the notch offset, and the crack always grows toward the top-loading head. When the notch offset is 0 mm, the vertical load applies at the loading head, and the crack grows upward along the line between the crack tip and the loading head. When the notch offset is greater than 0 mm, the crack expands upward toward the loading head, but the crack propagation directions form a certain angle with the connecting line between the loading head and the crack tip. The fracture angle (the included angle between the direction of crack growth and the direction of the pre-notch) of the specimen varies with the notch offset, as shown in Fig. 9. In this paper, when the offset distance increases from 0 to 72 mm, the mean fracture angle of the specimens increases by 16.96°-25.25°. It is noticeable that when the offset distance increases from 48 mm to 72 mm, the increase of fracture angle decreases, and even the mean fracture angle of the SC group decreases by 2.05°. But generally speaking, the fracture increases with the offset distance of the pre-notch in a certain range.

The deformation of brittle rock material can be understood as the relative displacement between mineral particles of rock, which reduces or loses the original ability to transmit force among particles. Therefore, it is feasible to use strain to characterize the ability of materials to resist mutual displacement between mineral particles. Compared with the stress intensity index, strain emphasizes that material failure is the result of force, so the physical meaning of strain as an intensity index is more intuitive. The crack germination first occurs at the tip of the pre-notch, and it is of great significance to evaluate the fracture resistance of the specimen by studying the maximum principal strain growth rate at the tip of the pre-notch. Hence, a region of 0.4 * 0.4 mm^2 at the notch tip was selected to conduct a quantitative study on its strain characteristics. The maximum principal strain at the tip of the pre-notch was taken as shown in Fig. 10a ~ d. The maximum principal strain at the tip is in a gentle growth stage for a period of time at the beginning, and the duration of this stage increases with the increase of notch offset. Until obvious cracks appear, the maximum principal strain at the tip suddenly increases. It can be seen that DC is more sensitive to cracks, and the maximum principal strain at the tip increases sharply earlier. In other words, the brittleness of dried sandstone is greater, and obvious cracks appear earlier and spread faster. High water content prolongs the process of fracture initiation and shortens the stage of fracture convergence and penetration.

In the study of pure mode I fracture, parameters such as crack opening displacement (COD) [42,43], crack tip opening displacement (CTOD) [44,45], and crack mouth opening displacement (CMOD) [46,47] are often used to characterize the displacement on both sides of the fracture surface of the specimen. All of them in the crack plane are usually considered as a linear distribution. In fact, when mixed mode I-II fracture occurs, the points on both sides of the crack surface have horizontal and vertical displacements after deformation, as shown in Fig. 11a. Aperture $\times$ (*apx*) and aperture *y* (*apy*) curves can be obtained by DIC to represent the vertical and horizontal displacements between two points, and then the curve of aperture (*ap*) can be obtained to represent the actual displacement in Fig. 11b. It is worth noting that the horizontal displacement of the crack tip is greater than the vertical displacement, which proves that the tensile fracture is the main part of the tension-shear fracture. To more intuitively understand the fracture process of sandstone specimens near the pre-notch under TPB, another three test locations near the pre-notch, namely Test location #1, Test location #2, and Test location #3, were designed on the specimen, as shown in Fig. 11c.

Changes in the *ap* of specimens with different conditions in the loading process, analyzed by DIC, as shown in Fig. 12. Point C is the peak load point, while point D is the unstable point of the *ap* value. The

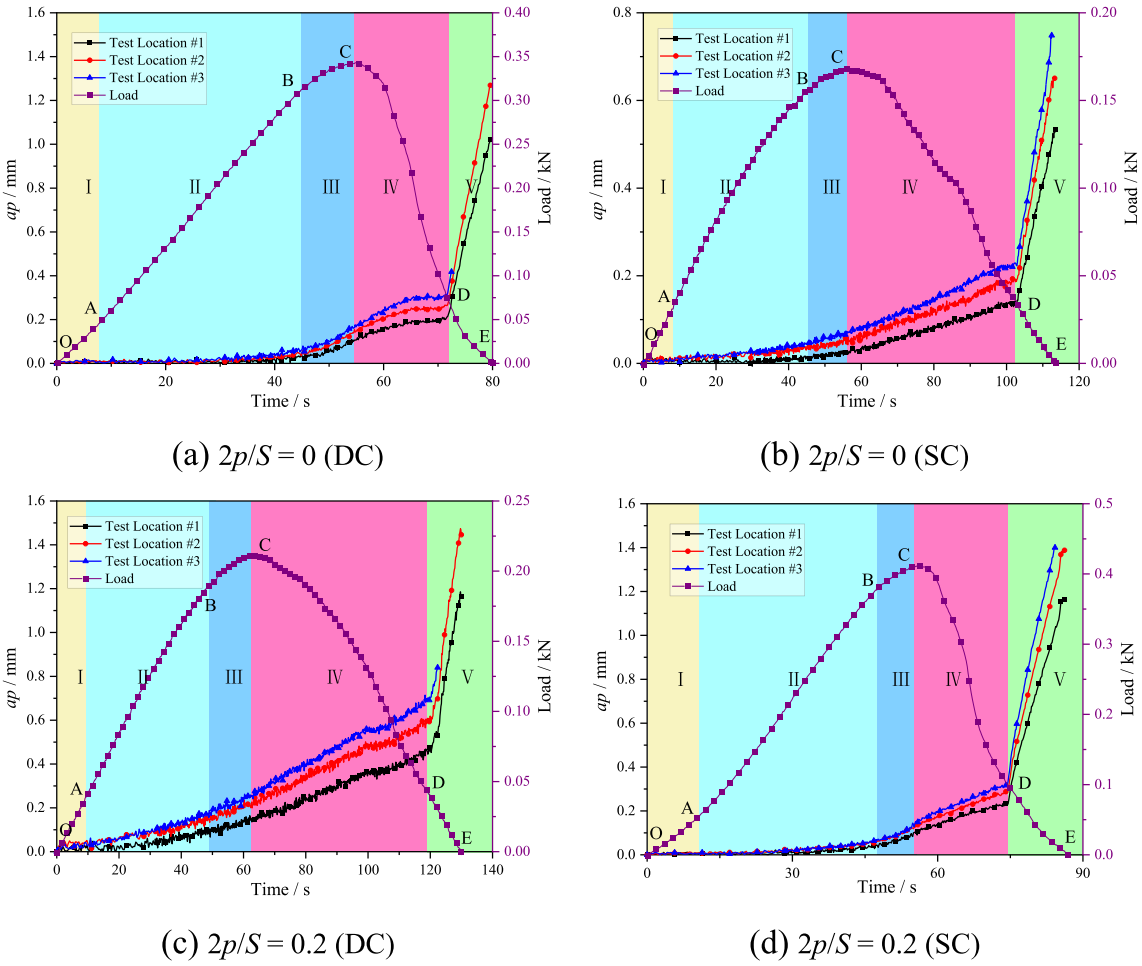

Fig. 12. Changes of the aperture of test location in the loading process analyzed by DIC.

unstable point indicates the critical point of unstable fracture. By comparing the ap values at different test locations, it can be found that the ap values at the test points farther from the crack tip are larger. Compared with the SC group, the DC group appears at an unstable point earlier. At the beginning of loading, the *ap* value of the test point is basically unchanged. As the crack occurs, the *ap* value of the test location increases approximately linearly. With the process of loading, the *ap* value of the specimen increases non-linearly and reaches the critical point of unstable fracture. After the unstable point, the specimen cracks propagate rapidly until the specimen is completely fractured.

Besides, according to the load-time curve, the fracture process can be divided into the compaction stage (I), the line elasticity stage (II), the microcrack propagation stage (III), the post-peak stable propagation stage (IV), and the post-peak unstable propagation stage (V). The compaction stage (OA) and line elasticity stage (AB) have been mentioned above. The BC segment is the microcrack propagation stage, the CD segment is the post-peak stable propagation stage, and the DE segment is the post-peak unstable propagation stage. In the microcrack growth stage, obvious stress concentration occurs at the crack tip. The primary crack in the rock begins to expand, and the secondary crack begins to germinate and propagate in this stage. Furthermore, the variation of the *ap* value of saturated sandstone at this stage is less than that of dried sandstone, which may be due to the pore water pressure in the microcrack and Stefan effect [5], which hinders the propagation of the microcrack. For the post-peak macrocrack propagation stage, it is usually directly divided into the non-stable crack propagation stage. In this test, the displacement of the test points near the crack was quantitatively analyzed by DIC, and the post-peak stage was further divided into the post-peak stable propagation stage and the post-peak unstable propagation stage. In the post-peak stable propagation stage, the *ap* value of the test point grows slowly, while it increases almost linearly and rapidly in the post-peak unstable propagation stage.

4. Conclusions

In this work, the digital image correlation (DIC) method was applied to study fracture and deformation behaviors of saturated and dried single-edge notched beam (SENB) sandstone under three-point bending (TPB) tests. Three moisture conditions (natural condition, saturated condition, and dried condition) and four notch offsets (0 mm, 24 mm, 48 mm, and 72 mm) were considered. The fracture behavior was interpreted by analyzing the change in peak load, fracture toughness, maximum principal strain field, and the aperture of pre-notch. Some key conclusions regarding the fracture and deformation behavior of the saturated and dried SENB sandstones are summarized as follows:

(1) The peak load of sandstone is affected by moisture condition and the fracture mode of pre-notch. The peak load of sandstone is more affected by fracture mode. In this paper, the average peak load of dried sandstone is 42.18–116.08% higher than that of saturated sandstone. By increasing the offset distance of the pre-notch (0–72 mm), the specimen is transformed from pure mode I fracture to mixed mode I-II fracture, and the average peak load of the specimen increased by 152.83%-284.24%.
(2) The water in sandstone weakens the ability of sandstone to resist fracture, and the effective fracture toughness of sandstone is also

affected by the fracture mode of pre-notch. In this paper, when the pure mode I fracture occurs in saturated sandstone, the fracture toughness is 66.74% of that natural sandstone, which is 46.28% of that dried sandstone. The effective fracture toughness of sandstone with consistent moisture condition under the mixed mode I-II load is 1.05–1.70 times that of the pure mode I load. The fracture toughness of saturated sandstone is most significantly affected by the loading mode. When the offset distance of pre-notch increases from 0 to 72 mm, the average effective fracture toughness increases from 4.324 MPa·mm$^{0.5}$ to 7.357 MPa·mm$^{0.5}$, increasing by 70.14%.

(3) Different from the common parameters such as crack opening displacement (COD), crack tip opening displacement (CTOD), and crack mouth opening displacement (CMOD), the aperture was used to characterize of the opening degree of the pre-notch in this paper. The value of pre-notch aperture *ap* in the fracture process is calculated by DIC. Consider the inflection point of the abrupt increase in *ap* value as the unstable point. The post-peak macroscopic crack propagation is divided into post-peak stable point propagation stage and post-peak unstable propagation stage by the unstable point.

Additionally, considering the existence of cracks in practical engineering, it is often not a single existence, but several cracks that exist at the same time. Therefore, to further understand the fracture and deformation behavior of rock with cracks under different moisture conditions in practical engineering, we will continue to study the fracture and deformation behavior of sandstone with several prefabricated cracks under different moisture conditions.

CRediT authorship contribution statement

Xiaofeng Qin: Writing – original draft, Investigation, Formal analysis, Data curation. **Haijian Su:** Writing – original draft, Visualization, Funding acquisition. **Yujie Feng:** Methodology, Funding acquisition. **Honghui Zhao:** Data curation, Resources, Writing – review & editing. **Nhan Pham Thi:** Writing – review & editing.

Declaration of Competing Interest

The authors declare that they have no known competing financial interests or personal relationships that could have appeared to influence the work reported in this paper.

Acknowledgments

This study is financed by the National Natural Science Foundation of China (Nos. 42077240, 51704279) and the Graduate Research and Innovation Projects in Jiangsu province (No. KYCX21_2279).

References

[1] Q. Yao, T. Chen, M. Ju, S. Liang, Y. Liu, X. Li, Effects of water intrusion on mechanical properties of and crack propagation in coal, Rock Mech. Rock Eng. 49 (12) (2016) 4699–4709.
[2] Y.T. Zhang, X.L. Ding, S.L. Huang, Y.J. Wu, J. He, Strength degradation of a natural thin-bedded rock mass subjected to water immersion and its impact on tunnel stability, Geomechanics and Engineering 21 (1) (2020) 63–71.
[3] D. Li, L.N.Y. Wong, G. Liu, X. Zhang, Influence of water content and anisotropy on the strength and deformability of low porosity meta-sedimentary rocks under triaxial compression, Eng. Geol. 126 (2012) 46–66.
[4] K. Hashiba, K. Fukui, Effect of water on the deformation and failure of rock in uniaxial tension, Rock Mech. Rock Eng. 48 (5) (2015) 1751–1761.
[5] Z. Zhou, X. Cai, W. Cao, X. Li, C. Xiong, Influence of water content on mechanical properties of rock in both saturation and drying processes, Rock Mech. Rock Eng. 49 (8) (2016) 3009–3025.
[6] Z.A. Erguler, R. Ulusay, Water-induced variations in mechanical properties of clay-bearing rocks, Int. J. Rock Mech. Min. Sci. 46 (2) (2009) 355–370.
[7] P.H.S.W. Kulatilake, B. Malama, J. Wang, Physical and particle flow modeling of jointed rock block behavior under uniaxial loading, Int. J. Rock Mech. Min. Sci. 38 (5) (2001) 641–657.
[8] L.N.Y. Wong, H.H. Einstein, Systematic evaluation of cracking behavior in specimens containing single flaws under uniaxial compression, Int. J. Rock Mech. Min. Sci. 46 (2) (2009) 239–249.
[9] Y.-H. Huang, S.-Q. Yang, M.R. Hall, W.-L. Tian, P.-F. Yin, Experimental study on uniaxial mechanical properties and crack propagation in sandstone containing a single oval cavity, Archives of Civil and Mechanical Engineering 18 (4) (2018) 1359–1373.
[10] X. Xi, X.u. Wu, Q. Guo, M. Cai, Experimental investigation and numerical simulation on the crack initiation and propagation of rock with pre-existing cracks, IEEE Access 8 (2020) 129636–129644.
[11] S.-Q. Yang, H.-W. Jing, Strength failure and crack coalescence behavior of brittle sandstone samples containing a single fissure under uniaxial compression, Int. J. Fract. 168 (2) (2011) 227–250.
[12] Liu Z L, Ma C D, Wei X A, Xie W B. Experimental study on mechanical properties and failure modes of pre-existing cracks in sandstone during uniaxial tension/compression testing. Engineering Fracture Mechanics, 2021, 255: article no. 107966.
[13] W. Wang, Y.X. Zhao, T. Teng, C. Zhang, Z.H. Jiao, Influence of bedding planes on mode I and mixed mode (I-II) dynamic fracture toughness of coal: analysis of experiments, Rock Mech. Rock Eng. 54 (1) (2021) 173–189.
[14] S.M.J. Razavi, M.R.M. Aliha, F. Berto, Application of an average strain energy density criterion to obtain the mixed mode fracture load of granite rock tested with the cracked asymmetric four-point bend specimens, Theroetical and Applied Fracture Mechanics 97 (2018) 419–425.
[15] S. Miao, P.-Z. Pan, Z. Wu, S. Li, S. Zhao, Fracture analysis of sandstone with a single filled flaw under uniaxial compression, Eng. Fract. Mech. 204 (2018) 319–343.
[16] L.N.Y. Wong, H.H. Einstein, Crack coalescence in molded gypsum and carrara marble: Part 1. Macroscopic observations and interpretation, Rock Mech. Rock Eng. 42 (3) (2009) 475–511.
[17] M. Sagong, A. Bobet, Coalescence of multiple flaws in a rock-model material in uniaxial compression, Int. J. Rock Mech. Min. Sci. 39 (2) (2002) 229–241.
[18] C.H. Park, A. Bobet, Crack initiation, propagation and coalescence from frictional flaws in uniaxial compression, Eng. Fract. Mech. 77 (14) (2010) 2727–2748.
[19] S. Miao, P.-Z. Pan, S. Zhao, J. Han, P. Konicek, A new DIC-based method to identify the crack mechanism and applications in fracture analysis of red sandstone containing a single flaw, Rock Mech. Rock Eng. 54 (8) (2021) 3847–3871.
[20] L. Liu, H. Li, X. Li, D.i. Wu, G. Zhang, Underlying mechanisms of crack initiation for granitic rocks containing a single pre-existing flaw: insights from digital image correlation (DIC) analysis, Rock Mech. Rock Eng. 54 (2) (2021) 857–873.
[21] Z. Yue, Y. Song, P. Li, S. Tian, X. Ming, Z. Chen, Applications of digital image correlation (DIC) and the strain gage method for measuring dynamic mode I fracture parameters of the white marble specimen, Rock Mech. Rock Eng. 52 (11) (2019) 4203–4216.
[22] S.T. Miao, P.Z. Pan, X.G. Zhao, C.Y. Shao, P.Y. Yu, Experimental study on damage and fracture characteristics of Beishan granite subjected to high-temperature treatment with DIC and AE techaniques, Rock Mech. Rock Eng. 54 (2) (2021) 721–743.
[23] I. Artamendi, H.A. Khalid, A comparison between beam and semi-circular bending fracture tests for asphalt, Road Materials and Pavement Design 7 (sup1) (2006) 163–180.
[24] M.R. Ayatollahi, J. Akbardoost, Size and geometry effects on rock fracture toughness: mode I fracture, Rock Mech. Rock Eng. 47 (2) (2014) 677–687.
[25] Q. Rao, Z. Sun, O. Stephansson, C. Li, B. Stillborg, Shear fracture (mode II) of brittle rock, Int. J. Rock Mech. Min. Sci. 40 (3) (2003) 355–375.
[26] J. Bidadi, J. Akbardoost, M.R.M. Aliha, Thickness effect on the mode III fracture resistance and fracture path of rock using ENDB specimens, Fatigue Fract. Eng. Mater. Struct. 43 (2) (2020) 277–291.
[27] Y. Luo, L. Ren, L.Z. Xie, T. Ai, B. He, Fracture behavior Investigation of a typical sandstone under mixed-mode I/II loading using the notched deep beam bending method, Rock Mech. Rock Eng. 50 (8) (2017) 1987–2005.
[28] L.G. Tham, H. Liu, C.A. Tang, P.K.K. Lee, Y. Tsui, On tension failure of 2-D rock specimens and associated acoustic emission, Rock Mech. Rock Eng. 38 (1) (2005) 1–19.
[29] H.P. Xie, Y. Ju, L.Y. Li, Criteria for strength and structural failure of rocks based on energy dissipation and energy release principles, Chinese Journal of Rock Mechanics and Engineering 24 (17) (2005) 3003–3010 (in Chinese).
[30] H.P. Xie, J. Yang, L.Y. Li, R.D. Peng, Energy mechanism of rock mass deformation and failure process, Chinese Journal of Rock Mechanics and Engineering 27 (9) (2008) 1729–1740 (in Chinese).
[31] Z. Liu, J. Shao, S. Xie, N. Conil, W. Zha, Effects of relative humidity and mineral compositions on creep deformation and failure of a claystone under compression, Int. J. Rock Mech. Min. Sci. 103 (2018) 68–76.
[32] D.C. Zhang, R.P. Gamage, M.S.A. Perera, C.P. Zhang, W.A.M. Wanniarachchi, Influence of water saturation on the mechanical behavior of low-permeability reservoir rocks, Energies 10(2), article no. 236 (2017).
[33] M.O. Ciantia, R. Castellanza, C. di Prisco, Experimental study on the water-induced weakening of calcarenites, Rock Mech. Rock Eng. 48 (2) (2015) 441–461.
[34] Y. Nara, M. Tanaka, T. Harui, Evaluating long-term strength of rock under changing environments from air to water, Eng. Fract. Mech. 178 (2017) 201–211.
[35] T. Fett, Mixed-mode Stress intensity factors for three-point bending bars, Int. J. Fract. 48 (4) (1991) R67–R74.
[36] H.F. Deng, Z. Wang, J.L. Li, Q. Jiang, H.B. Zhang, Experimental research about influence of low pore water pressure on unloading mechanical properties of

sanstone, Chinese Journal of Rock Mechanics and Engineering 36 (S1) (2017) 3266–3275 (in Chinese).
[37] Z.S. Lou, J.L. Li, Q. Jiang, Y.C. Zhang, Y.S. Huang, E. Assefa, H.F. Deng, Effect of the water-rock interaction on the creep mechanical properties of the sandstone rock, Periodica Polytechnica Civil Ebfineering 62 (2) (2018) 451–461.
[38] Jeng F S, Lin M L, Huang T H. Wetting deterioration of soft sandstone-microscopic insights. An International Conference on Geotechnical and Geological Engineering, 2000, Melbourne.
[39] Huang F, Wu C Z, Ni P P, Wan G Q, Zheng A C, Jang B A, Karekal S. Experimental analysis of progressive failure behavior of rock tunnel with a fault zone using non-contact DIC technique. International Journal of Rock Mechanics and Mining Sciences, 2020, 132, article no. 104355.
[40] J. Hosdez, M. Langlois, J.-F. Witz, N. Limodin, D. Najjar, E. Charkaluk, P. Osmond, A. Forre, F. Szmytka, Plastic zone evolution during fatigue crack growth: Digital image correlation coupled with finite elements method, Int. J. Solids Struct. 171 (2019) 92–102.
[41] H. Song, H. Zhang, D. Fu, Q. Zhang, Experimental analysis and characterization of damage evolution in rock under cyclic loading, Int. J. Rock Mech. Min. Sci. 88 (2016) 157–164.
[42] H. Zhang, D. Fu, H. Song, Y. Kang, G. Huang, G. Qi, J. Li, Damage and fracture investigation of three-point bending notched sandstone beams by DIC and AE techniques, Rock Mech. Rock Eng. 48 (3) (2015) 1297–1303.
[43] B. Liu, Y.-T. Gao, A.-B. Jin, D. Elmo, Fracture characteristics of Orebody rock with varied grade under dynamic Brazilian tests, Rock Mech. Rock Eng. 53 (5) (2020) 2381–2398.
[44] Y. Wang, X. Hu, Determination of tensile strength and fracture toughness of granite using notched three-point-bend samples, Rock Mech. Rock Eng. 50 (1) (2017) 17–28.
[45] Cui P F, Guo W L. Crack tip opening displacement based description of three-dimensional creep crack border stress fields for partially penetrating cracked specimens. Engineering Fracture Mechanics, 2021, 241, article no. 107425.
[46] M.E. Arslan, Effects of basalt and glass chopped fibers addition on fracture energy and mechanical properties of ordinary concrete: CMOD measurement, Constr. Build. Mater. 114 (2016) 383–391.
[47] P. Moore, A. Pargeter, Comparison of using the crack mouth displacement (CMOD) and load line displacement (LLD) methods in the determination of critical J integral in SENB specimens, Fatigue Fract. Eng. Mater. Struct. 41 (9) (2018) 1997–2009.